

35. LITHOLOGIC CONTROL OF PHYSICAL-PROPERTY INTERRELATIONSHIPS¹

D. C. Nobes,² J. Mienert,³ and G. J. Dirksen⁴

ABSTRACT

The lithology of sediment sequences has a significant effect on the interrelationships of physical properties. Conversely, physical-property interrelationships can be diagnostic of the lithology and lithologic variations, of tectonic effects, and of depositional hiatuses. The physical-property measurements obtained on Leg 114 of the Ocean Drilling Program show correlations that are strongly dependent on the carbonate content, the biogenic silica (opal) content, and the presence of diagenetic cementation. The wet-bulk and grain densities in particular are indicative of silica vs. carbonate content: the greater the carbonate content, the greater the density becomes. The porosity and acoustic velocity are sensitive to diagenesis, and in the case of Leg 114 specifically illustrate the effects of carbonate diagenesis. As the carbonate content increases, the porosity decreases and the acoustic velocity correspondingly increases; as the degree of diagenesis increases, the porosity decreases and the acoustic velocity increases. The acoustic velocity follows a smooth progression along a theoretical model curve from ooze to chalk to limestone.

INTRODUCTION

Bulk physical properties are dependent on lithologic variations. The wet-bulk density, for example, is dependent on the porosity (the amount of pore fluid present) and on the grain density (the grain matrix material) (Johnson and Olhoeft, 1984). The acoustic velocity is dependent on the porosity and on the grain material, for example, the carbonate and clay contents (Hamilton et al., 1982; Mienert, 1984; Mienert et al., in press; Nobes et al., 1986; Nobes, 1989). We thus expect to see significant differences between carbonate-rich and silica-rich material. The physical properties, however, can be diagnostic of diagenetic effects as well. By that we mean not merely the decrease of porosity with increasing compaction but also the cementation of the solids, for example, carbonate dissolution and precipitation. In addition, tectonism and depositional hiatuses affect physical-property variations.

We examine the physical properties of the sediments recovered on Ocean Drilling Program (ODP) Leg 114. Sites 698 through 704 form a transect across the subantarctic South Atlantic (Figs. 1 and 2). Calcareous and nannofossil ooze, chalk, and limestone make up the majority of the sediments, and at Sites 699 and 700, in particular, an almost complete diagenetic sequence of calcareous ooze, chalk, and limestone was recovered (Fig. 2). Siliceous ooze is common at shallower depths, which influences the physical-property profiles. The effects of both erosional and nondepositional hiatuses are recorded by the physical properties, and the results from Leg 114 provide prototypical profiles.

PHYSICAL-PROPERTY METHODOLOGY

To place the discussion in context, we will outline the measurement and analysis techniques used to derive the physical properties. In particular, the sources of error will be identified. Once the physical-property methodology has been presented, we will discuss each set of physical properties in turn, noting the contrasting effects of carbonate and silica content and the effects of diagenesis, tectonism, and hiatuses.

Index Properties

The index properties include porosity, water content, wet-bulk density, dry-bulk density, and grain density, and all are computed using ratios of weights and volumes. Each physical-property sample was taken from freshly split, relatively undisturbed core. The size of the samples ranged from 5 to 10 cm³. Soft sediments were sampled using a large syringe, more consolidated sediment samples consisted of discrete, relatively undisturbed "chunks," and samples from more lithified sediments were obtained from pieces cut from the core.

Each sample was transferred to a sample container that had been previously calibrated for weight and volume. The sample was then weighed using a Scitech balance with a resolution of ± 0.01 g and a repeatability of ± 0.04 g. The volume of the sample was then determined using a Penta Pycnometer as the difference between the calibrated volume of the empty pycnometer cell and the volume with the sample present. The volume precision was $\pm 10^{-4}$ cm³ and was repeatable to ± 0.05 cm³. The relative error in the volume was greater than the relative error in the weight, so that calculations using the weights alone had smaller inherent errors.

The samples were then oven dried at 100°C for 24 hr. The dried samples were weighed and their volumes measured again. The index properties were computed using the procedure outlined by Boyce (1976). For Leg 114 Sites 701 through 704, the porosity was computed using an alternative equation that has been shown to be more valid (Mienert, 1986) because the more accurate weights are used, as opposed to the volumes. The effect on the porosity is small, amounting to at most a decrease of 3%.

¹ Ciesielski, P. F., Kristoffersen, Y., et al., 1991. *Proc. ODP, Sci. Results*, 114: College Station, TX (Ocean Drilling Program).

² Department of Earth Sciences and Department of Physics, University of Waterloo, Waterloo, Ontario, Canada N2L 3G1.

³ GEOMAR, Forschungszentrum der Christian-Albrechts-Universität zu Kiel, D-2300 Kiel, FRG.

⁴ Geological Engineering Program, University of Waterloo, Waterloo, Ontario, Canada N2L 3G1 (Present address: Department of Civil Engineering, University of Waterloo, Waterloo, Ontario, Canada N2L 3G1).

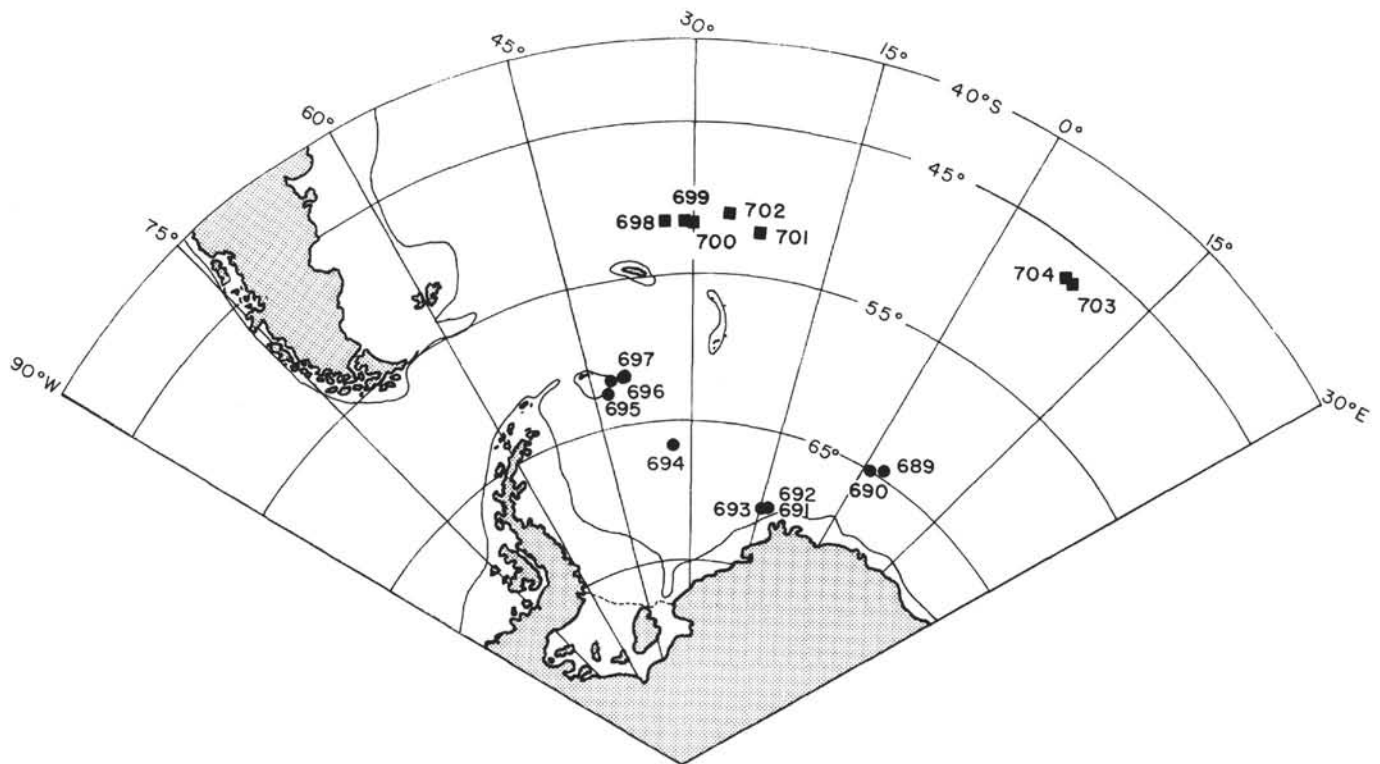


Figure 1. ODP Leg 113 (circles) and Leg 114 (squares) sites in the South Atlantic sector of the Southern Ocean. The seven sites drilled during ODP Leg 114 form a west-to-east transect across the subantarctic South Atlantic. (From Shipboard Scientific Party, 1988a.)

After correcting for the weight and volume of the sample container, we obtain the wet and dry weights as

$$\begin{aligned} \text{wet weight} &= \text{weight of seawater} + \text{weight of solid, and} \\ \text{dry weight} &= \text{weight of solid} + \text{weight of salt residue.} \end{aligned}$$

The difference between the wet and dry weights is the weight of the seawater minus the weight of the salt contained in the water. If we assume a salinity of 3.5%, then

$$\text{weight of seawater} = (\text{wet weight} - \text{dry weight}) / 0.965,$$

and the salt weight is determined as

$$\begin{aligned} \text{salt weight} &= \text{weight of seawater} \\ &- (\text{wet weight} - \text{dry weight}). \end{aligned}$$

The weight of the grain (solid) fraction is thus

$$\text{grain weight} = \text{dry weight} - \text{salt weight}.$$

The errors in the weights thus include not only the error in the balance reading, which propagates through all of the preceding differences and sums, but also our assumption of 3.5% salinity. As it turns out, that has a negligible effect compared to the error in the weights. The outlined calculation of the weights was laid out in that form for the data analysis. Although combinations of the equations could lead to simplifications, such combinations were not used in the computer

programs provided aboard ship. The errors cited are derived using the "reading errors," approximately equivalent to two standard deviations (or ~95% confidence level). The final errors in the weights are ± 0.04 g for the wet weight, ± 0.06 g for the weight of seawater, ± 0.08 g for the salt weight, and ± 0.09 g for the grain weight.

If we use an average salt density of 2.257 g/cm^3 (R. E. Boyce, unpubl. data), then we may compute the salt volume from the salt weight as

$$\text{salt volume} = \text{salt weight} / 2.257.$$

The grain volume is determined to be

$$\text{grain volume} = \text{dry volume} - \text{salt volume},$$

and the seawater volume is

$$\text{seawater volume} = \text{seawater weight} / 1.0245,$$

where the density of seawater is taken to be 1.0245 g/cm^3 based on the density of salt from Boyce (1976). The errors in the computed volumes all depend on the weights and are $\pm 0.04 \text{ cm}^3$ for the seawater volume and (at least) $\pm 0.06 \text{ cm}^3$ for the grain volume. The error in the seawater density is negligible in comparison, and the error in the salt density is undetermined.

From the weights and volumes we may then compute the index properties. The water content is simply

$$\text{water content} = \frac{\text{weight of seawater}}{\text{wet weight}} \times 100\%.$$

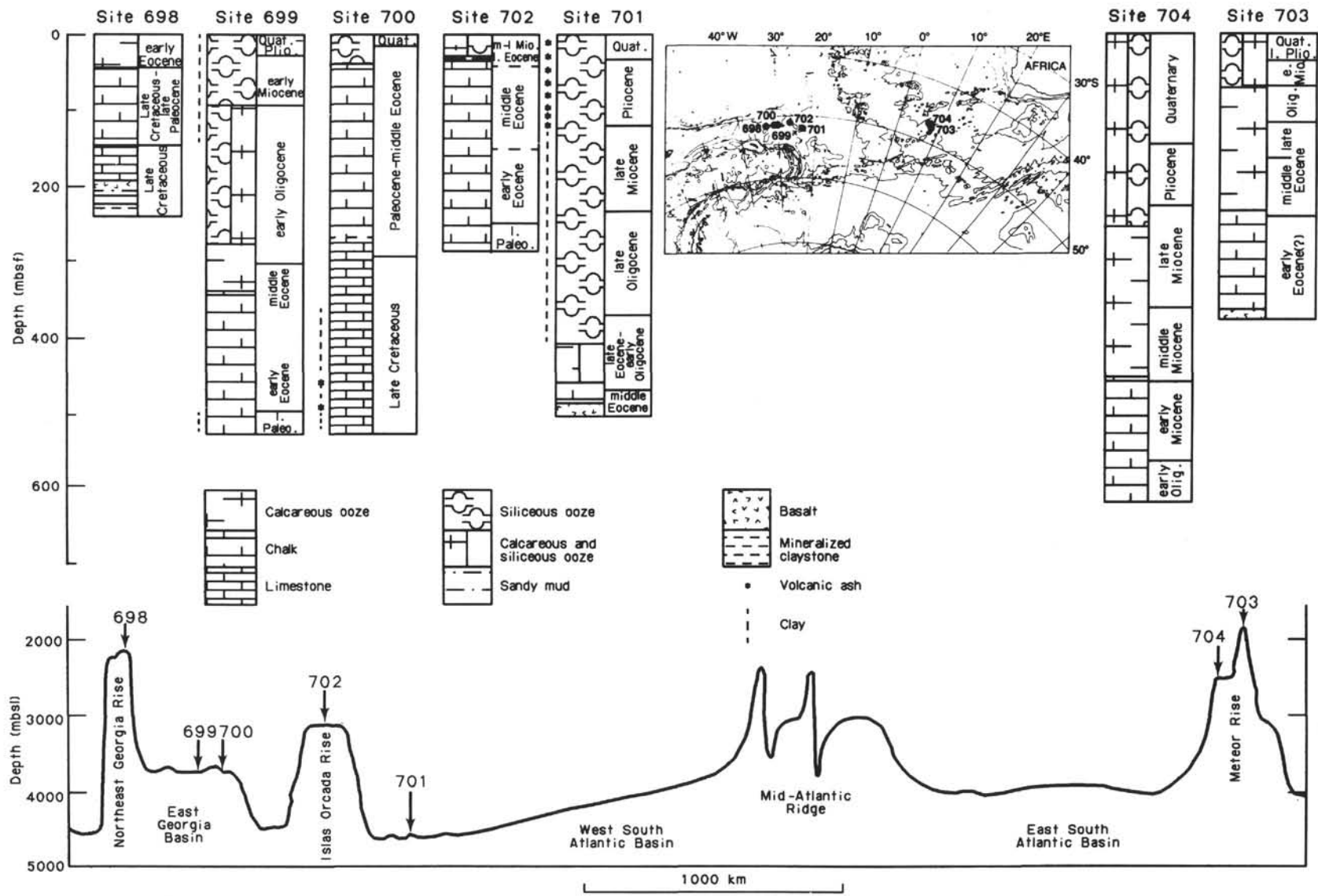


Figure 2. Composite stratigraphy columns (top) reveal the age, lithology, and sediment thickness of each Leg 114 site. A schematic cross section (bottom) shows the site locations along the bathymetry of the transect. Depth in meters below seafloor (mbsf). (From Shipboard Scientific Party, 1988a.)

The water content is generally expressed as a percentage between 0 and 100. Note that an alternative definition

$$\text{water content} = \text{weight of seawater} / \text{grain weight}$$

has often been used. This yields a value that is unbounded as the solid fraction approaches zero and, in addition, will have a larger error because the grain weight has a larger error associated with it. We prefer to use the first definition of water content, called "wet water content," because it is consistent with the standard definition of porosity

$$\text{porosity} = \frac{\text{seawater volume}}{\text{wet volume}} \times 100\%.$$

The alternate definition of water content, called the "dry water content," is more in keeping with the void ratio, which is defined as

$$\text{void ratio} = \text{volume of seawater} / \text{grain volume}.$$

The wet water content and porosity form a logical pair:

$$\begin{aligned} \text{porosity} &= (\text{seawater volume} / \text{wet volume}) \times 100\%, \text{ and} \\ \text{water content} &= (\text{seawater weight} / \text{wet weight}) \times 100\%, \end{aligned}$$

and the dry water content and void ratio form a second separate logical pair:

$$\begin{aligned} \text{void ratio} &= \text{seawater volume} / \text{grain volume}, \text{ and} \\ \text{water content} &= \text{seawater weight} / \text{grain weight}. \end{aligned}$$

In all of our discussions, we will use the wet water content and porosity. The errors in the porosity, void ratio, and water contents depend on the relative errors in the measurements. Using the largest relative errors for the volumes and weights (i.e., using the errors associated with the smallest samples), we find that the relative errors for wet water content and porosity are of the order of 20% for low-porosity rock chunks and a few percent for high-porosity samples. The relative errors remain high (of the order of 10% to 20%) for dry water content and void ratio even for soft sediments because the solid fraction is small and the relative errors in the dry properties become large.

The densities are calculated from the weights and volumes as follows:

$$\begin{aligned} \text{wet-bulk density} &= \text{wet weight} / \text{wet volume}, \\ \text{dry-bulk density} &= \text{grain weight} / \text{wet volume}, \text{ and} \\ \text{grain density} &= \text{grain weight} / \text{grain volume}. \end{aligned}$$

Based on our preceding error analyses, the relative errors are smallest for the wet-bulk density, of the order of a few percent or less, and largest for the grain density, from a low of about 7% to a high of as much as 15% for the samples with the highest porosities.

For Sites 698 to 700, a volume-based definition of porosity was used:

$$\text{porosity} = \frac{\text{wet volume} - \text{grain volume}}{\text{wet volume}} \times 100\%.$$

An alternative definition of porosity used for Sites 701 through 704 has the form

$$\text{porosity} = \frac{(\text{weight of seawater} / 1.0245) / 0.965}{\text{wet volume}} \times 100\%.$$

The relative errors are comparable when a detailed analysis is performed, but Mienert (1986) suggested that the alternative definition of porosity is more valid because it is based on the more accurate weights rather than the volumes. The difference between the two definitions of porosity was found to be at most 3% and could be used as a check of the internal consistency of the measurements.

We have so far discussed direct measurement error, but there are other potentially greater errors associated with the measurement process. This is illustrated by examining the plot of wet-bulk density vs. porosity (Fig. 3). The data values quite clearly follow a linear trend, but the average grain density as determined for the complete data set yields the straight line shown. There is an obvious and systematic discrepancy between the line and the data trend. The explanation is found by examining the effects of air drying of the samples between weighing and volume measurement. There is always some, usually small, delay between weighing a sample and measuring the volume. During the delay, air drying of the surface can remove water; the greater the surface area relative to the sample volume, the greater the relative drying. The effects should increase as the sample size decreases and will be greatest for the small samples. This is exactly the trend observed.

The air drying will remove water, thus reducing the volume occupied in the pycnometer by the wet sample. The reduced wet volume will thus lead to an increased wet-bulk density and

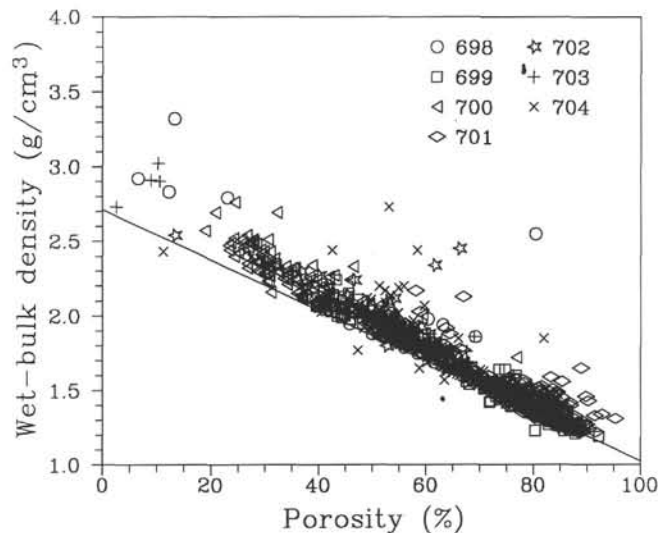


Figure 3. Wet-bulk density vs. porosity. The solid line represents the mixing model relating the wet-bulk density to the porosity for the average grain density of 2.71 g/cm³ for the complete Leg 114 data set. The deviation between the model and data increases with decreasing porosity (increasing density).

to an increased porosity. We can compute corrected values for the porosity (in %) and wet-bulk density, and find that

$$\phi_C = \phi - \delta\phi \text{ and } d_{bC} = d_b - \delta d_b,$$

where ϕ is the porosity, ϕ_C is the corrected porosity, d_b is the wet-bulk density, and d_{bC} is the corrected bulk density.

The correction terms $\delta\phi$ and δd_b are of the form

$$\delta\phi = a\phi + b \text{ and } \delta d_b = c\phi + d,$$

where $a = (-1.1 \pm 0.7) \times 10^{-3}$, $b = 0.28 \pm 0.19$, $c = (-1.05 \pm 0.46) \times 10^{-3}$, and $d = 0.18 \pm 0.12$ were determined using regression. The general trend is quite obvious and systematic, but the correction terms are small for any given pair of data values and are within the error limits. Thus, all analyses were performed using uncorrected data.

Thermal Conductivity

The thermal conductivity measurements were made at least once per core using a needle probe method (von Herzen and Maxwell, 1959). Briefly, a needle containing a heating wire and a thermistor was inserted through the liner into a whole-core section. A heat pulse was applied to the wire, which propagates into the core at a rate determined by the thermal conductivity. The thermistor was used to measure the decay rate of the heat pulse. The measurements were controlled by a Thermcon unit connected to a microcomputer that computed the thermal conductivity from the decay curve. The measurement time was 4 min. Calibration runs were made as often as possible with acceptable results. The SI units for thermal conductivity are watts/meter-Kelvin (W/m-K).

Because any discrepancy between the core and laboratory temperatures would alter the heat pulse decay, the core was allowed to equilibrate for 3 hr. Even so, some error may well be present as a result of lack of total equilibration. By far the greatest contribution to any error, however, was due to core disturbance. In more indurated cores, the core may have split during needle insertion, in which case the needle probe would not have been in complete contact with the core and inaccurate measurements would result. In most such cases the thermal conductivity had an obviously anomalous low value, close to that for water, 0.6 W/m-K, and could be discarded. However, it is difficult to gauge how much error may be present in the other readings. In this and other discussions in this volume, only the apparently "normal" thermal conductivities have been used. That is, only thermal conductivities greater than the thermal conductivity for water were used.

Acoustic Velocity

Acoustic velocity measurements were taken using a Hamilton Frame (Boyce, 1976) in two different modes: for soft sediments, traveltimes were measured across the split core, including the core liner. Traveltimes were thus only recorded in one direction, perpendicular to the core. For lithified sediments, traveltimes were recorded for discrete samples. Acoustic traveltimes could be recorded in three perpendicular directions, if desired. The calibration and operating procedures were as outlined by Boyce (1976). The traveltimes were recorded by direct observation of the waveforms as displayed using an oscilloscope, which gives rise to errors in picking the first breaks.

No correction factors were applied to the velocities. After removal of time delays resulting from the liner, if

present, and the cable, calibration velocities agreed with accepted acoustic velocities for aluminum and lucite within an error of ± 50 m/s, including operator error. Because the traveltimes were read directly from the oscilloscope waveforms, the readings were susceptible to operator reading error. The errors in the velocities were thus estimated from comparisons of readings taken by the respective operators for the velocity standards. Tests on sample cubes cut from lithified core indicated that the velocities as determined by different operators were repeatable to within ± 20 m/s, and in one case to within ± 5 m/s.

Shear Strength

Vane-shear-strength measurements were made using the hand-held "Torvane" apparatus for Site 698. The remainder of the measurements for Sites 699 through 704 was made with the motorized vane shear system using a procedure similar to that described by Boyce (1977). No estimates of errors or repeatability were made.

It must be noted that the shear vane apparatus was designed for use with clayey sediments with shear strengths less than 100 kPa (Craig, 1983). Most of the sediments recovered on Leg 114 are calcareous or a mixture of calcareous and siliceous material. In addition, many of the shear strength values exceeded 100 kPa. Thus, strictly speaking, the shear vane measurements were not valid.

Other Techniques

Other physical-property data gathered were gamma-ray attenuation (GRAPE) density and *P*-wave logger (PWL) velocity. Those data are not discussed in any detail here, and the methodology will not be outlined. To summarize their concordance with the other physical-property data, we have noted a general correspondence between the GRAPE and wet-bulk densities. The variations are approximately the same, and the absolute values are similar. The PWL velocity does not generally appear to follow the other data closely, because of core disturbance resulting from the extended core barrel procedure and because of poor coupling of the transducers with the core liner, and the PWL data have not been used for any interpretation.

POROSITY

The carbonate content has a major controlling influence over the physical properties, as illustrated in the porosity vs. carbonate crossplot (Fig. 4). Note the general decrease in porosity with increasing carbonate content. Silica and clay minerals in general have higher porosities. Hamilton et al. (1982) noted a similar pattern in wet-bulk density vs. carbonate content. We can compare the relative effects of the silica and carbonate contents by examining the data from Site 704 (Fig. 5), where a regular sequence of glacial and interglacial cycles resulted in alternating silica- and carbonate-rich layers. The silica layers tend to have higher porosities than the carbonate layers. The effects of compaction and cementation with increasing depth are superimposed on the separation of the silica and carbonate samples. We will return to a consideration of the effects of the alternating silica and carbonate layers when we discuss the densities in the next section.

The effects of diagenetic compaction and cementation, in the form of micritic calcite, are most notable at the adjacent Sites 699 and 700 (Fig. 6). Note the trend, much as one might expect, of decreasing porosity with increasing degree of cementation, from ooze to chalk to limestone. As at the other sites, the highest porosities are encountered in the siliceous oozes recovered at shallower depths.

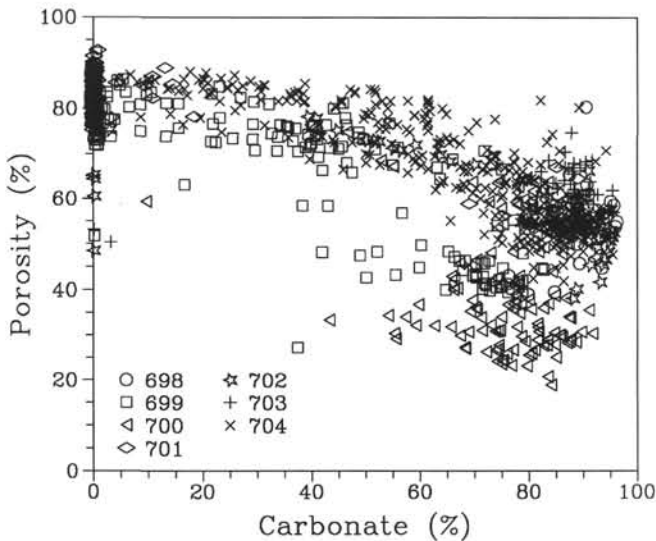


Figure 4. Porosity vs. carbonate content. Note the general trend of decreasing porosity with increasing carbonate content. Alternatively, we can define the trend as increasing porosity with an increase in the content of noncarbonate minerals, such as silica or clay minerals.

The data from Sites 699 and 700 also illustrate the effects of tectonic uplift and subsequent erosion. A composite plot of the physical properties vs. age is presented in Figure 7. The grain density and the carbonate content are the same in the overlapping sections, but the porosity at Site 700 is markedly less than at Site 699 for samples of comparable age. Two faults separate Sites 699 and 700, and Site 700 has been uplifted by as much as 550 m (Shipboard Scientific Party, 1988b). The material at Site 700 has not undergone as much compaction and cementation, as illustrated in Plate 1. SEM photomicrographs of samples of comparable age from Sites 699 and 700 show a marked difference in the degree of calcite overgrowth. The differences between the physical-property profiles, the porosity in particular, are diagnostic of the differences in the degree of diagenesis (e.g., van der Lingen and Packham, 1975).

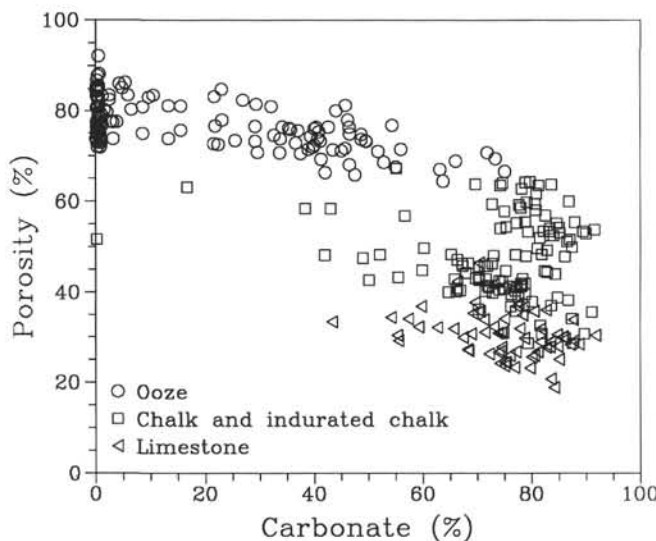


Figure 5. Porosity vs. carbonate content for Site 704 data only. The high porosities tend to be correlated with the siliceous ooze, and the lower porosities are correlated with the calcareous ooze and chalk.

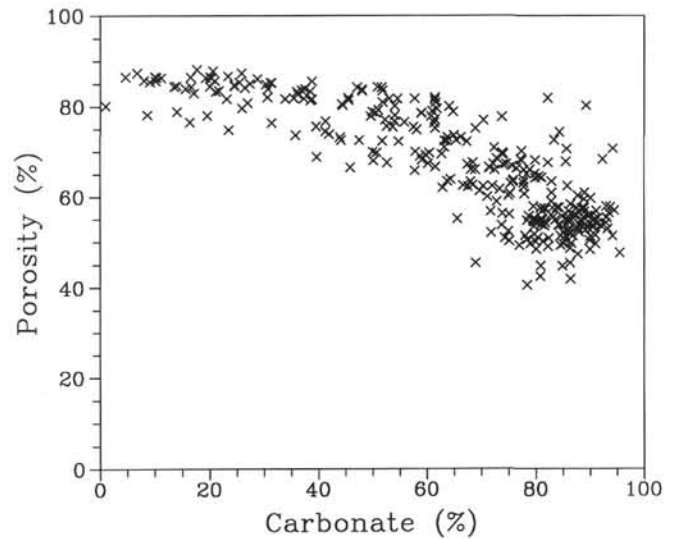


Figure 6. Porosity vs. carbonate content for Sites 699 and 700, showing the diagenetic trend of decreasing porosity as the sediments progress from ooze to chalk to limestone. The higher porosity values are associated with the shallow siliceous ooze of Site 699.

The physical properties, and again the porosity specifically, are affected by hiatuses in sediment deposition. Such hiatuses can arise because of erosion, resulting from uplift of the sediment or an increase in bottom water flow, or because of the lack of sediment deposition, a nondepositional hiatus. The porosity profiles for Holes 699A and 702A provide prototypes for the classification of the type of hiatus (Fig. 8). The slow deposition or lack of deposition of sediments provides an environment conducive to the formation of manganese nodules and mats. Thus, the presence of manganese in substantial amounts can confirm the occurrence of a nondepositional hiatus, as illustrated in the porosity profile from Hole 699A (Fig. 8A). The manganese mat may be a layer of limited permeability, limiting fluid flow through the mat, giving rise to an increase of porosity across the nondepositional hiatus. Erosional hiatuses, conversely, remove the upper layers of material that may have undergone some compaction. The layers removed are later replaced by less consolidated sediments, and the porosity decreases across an erosional hiatus, as exemplified by the Hole 702A porosity profile (Fig. 8B).

DENSITIES

Diagenetic cementation does not significantly affect the grain density, as we can see in Figure 9 for the grain density vs. carbonate content. There is a steady convergence of the grain density values on the carbonate grain density as the carbonate content increases. The grain density values are scattered for the samples low in carbonate content. Clay minerals have highly variable grain densities, but the most common forms (illite, kaolinite, and montmorillonite) have average grain densities, 2.6 to 2.7 g/cm³ (Johnson and Olhoeft, 1984), that are not much different from the Leg 114 average grain density, 2.71 ± 0.19 g/cm³. The basaltic samples have higher grain densities, and opal has low grain densities, of the order of 1.8 g/cm³ (Johnson and Olhoeft, 1984). When we separate the samples for Site 704 from the rest of the samples (Fig. 10), we can see a definite trend resulting from the presence of lower density siliceous material. The lithology of Site 704, especially in the upper sections, is dominated by carbonate and silica. The grain density for samples with carbonate content greater than 70% is 2.77 ± 0.13 g/cm³,

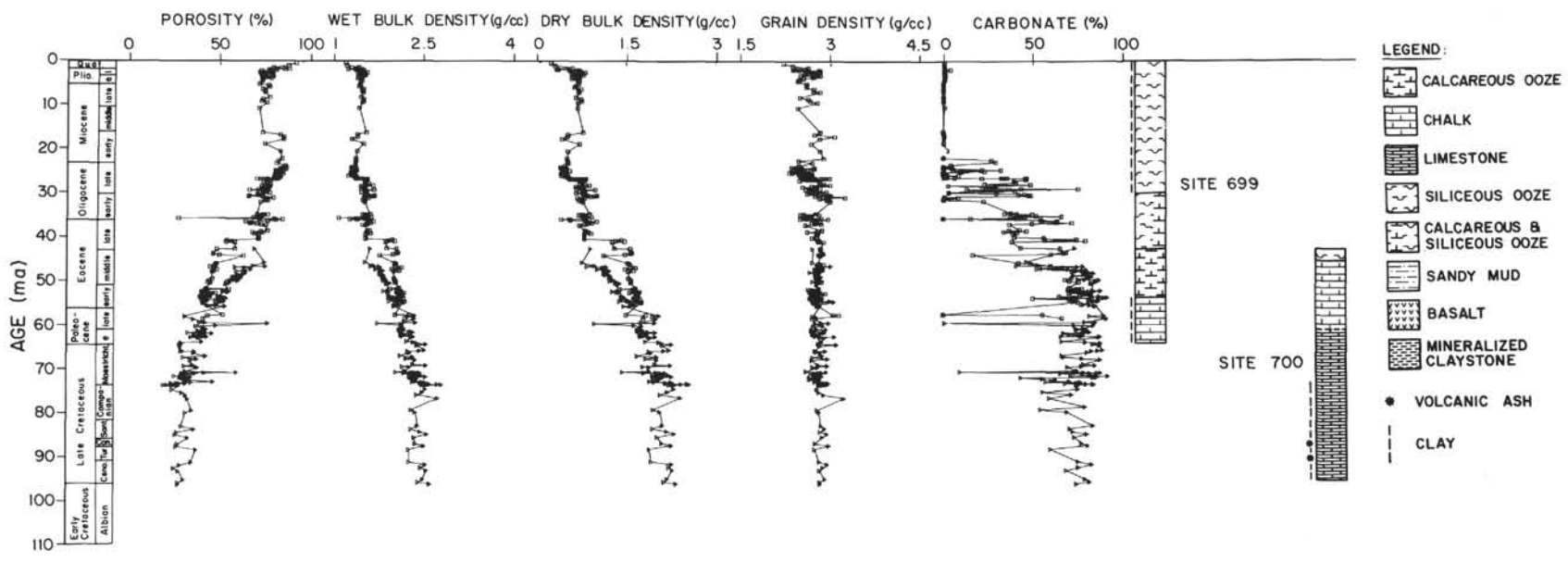


Figure 7. Physical properties vs. age for Sites 699 and 700. The lithologic columns are shown on the right for comparison. Note the offset between the porosity and bulk density data of comparable ages for the two sites.

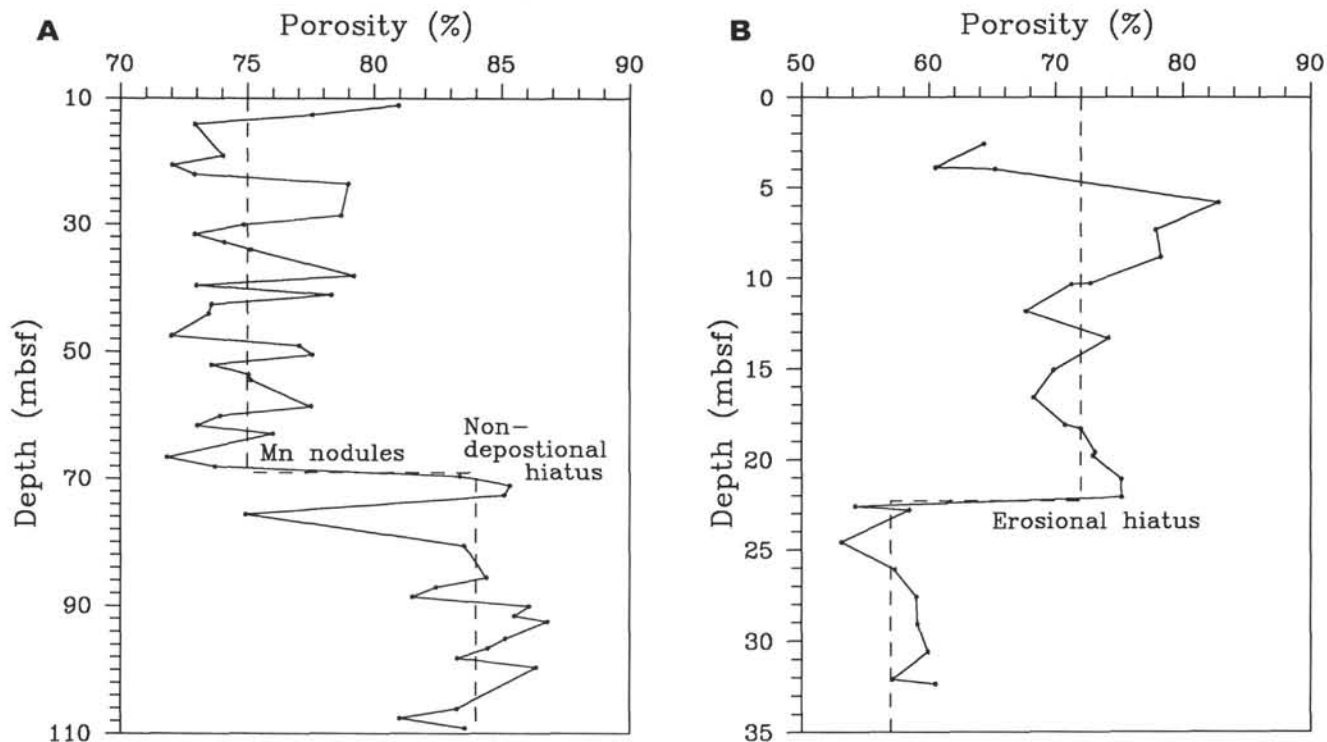


Figure 8. Two examples of porosity vs. depth, illustrating the change in porosity across depositional hiatuses. A. Nondepositional hiatus in Hole 699A at a depth of approximately 69 mbsf. A manganese mat and manganese nodules are present at and above the hiatus. Note the change in the average value of porosity across the hiatus. B. Erosional hiatus in Hole 702A at a depth of approximately 22.4 mbsf. Note the sharp decrease in porosity across the hiatus.

and it is $2.59 \pm 0.23 \text{ g/cm}^3$ for samples with a carbonate content less than 30%.

Another pattern emerges when we examine the variation of grain density with porosity (Fig. 11). The samples with a lower grain density, those rich in silica, tend to be the higher porosity samples. The silica-rich samples do not persist in the deeper sections. The upturn in the grain density at lower porosities is simply diagnostic of the basaltic samples, which have higher grain densities. The few high values of grain density at high porosities are due to mineralization, primarily manganese. As for the grain density vs. carbonate, the silica to carbonate trend is perhaps most clearly evident in the data for Site 704 alone (Fig. 12), where alternating layers of siliceous and calcareous oozes were recovered (e.g., the GRAPE density data for Core 114-704A-7H; Fig. 13). The combined effects of the high-porosity, low-grain-density siliceous oozes vs. the lower porosity, higher grain density calcareous oozes are readily distinguished.

THERMAL CONDUCTIVITY

The carbonate content has a significant effect on the thermal conductivity as well. The crossplot of thermal conductivity vs. porosity is shown in Figure 14, along with the theoretical curves derived using the geometric mean formula (Woodside and Messmer, 1961; Henderson and Davis, 1984) and the average grain thermal conductivities for the whole data set and for carbonate content greater than 70%. The geometric mean thermal conductivity is given as

$$\log k = (1 - \phi)\log k_g + \phi(\log k_w),$$

where ϕ is the porosity, k_g is the grain thermal conductivity, and k_w is the thermal conductivity of seawater, about 0.6

W/m-K. The mean grain thermal conductivity for Leg 114 is $6.8 \pm 5.0 \text{ W/m-K}$ whereas the mean k is $5.2 \pm 1.5 \text{ W/m-K}$ for samples with 70% carbonate content or greater. The results are substantially the same if we compute the mean logarithm of the grain thermal conductivity instead; the means are slightly different, but the maxima and minima are the same. Because there tends to be a correlation between lower porosity and higher carbonate content, as shown in Figure 3, we see a deviation from the theoretical curve at lower porosities, where the grain thermal conductivity of the carbonate dominates. The two geometric mean models, using the overall and the carbonate mean k_g , illustrate the increasing deviation of the models at the lower porosities and the excellent fit of the data to the model when the carbonate mean k_g is used.

How good is our value for the carbonate mean k_g ? The grain thermal conductivity is plotted vs. grain density in Figure 15 for carbonate-rich samples. Note the tight cluster of points centered about the mean values of grain density and grain thermal conductivity. For comparison, the overall Leg 114 mean values are shown with representative error bars. Contrast the tight cluster of data values for the carbonate-rich samples with the scatter of points for the noncarbonaceous samples (Fig. 16). Some of the samples are very silica-rich. We would like to obtain an estimate of the grain thermal conductivity of silica. However, the fluid, in this case seawater, so dominates the thermal conductivity at high porosities that estimates of the silica grain thermal conductivity from individual samples are necessarily suspect. The grain thermal conductivity for samples with less than 30% carbonate content, which is dominated by the silica-rich samples but includes lower grain thermal conductivities for clay-bearing sediments from Site 701, is $7.7 \pm 6.9 \text{ W/m-K}$. The effects of the higher silica grain thermal conductivity on heat flow will

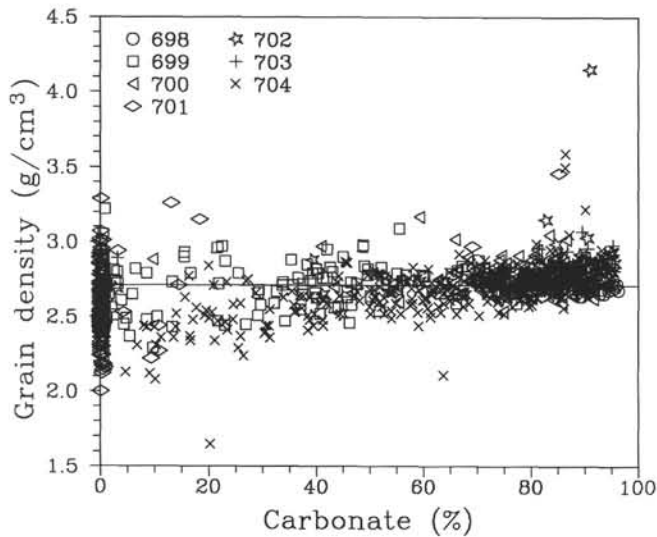


Figure 9. Grain density vs. carbonate content. The horizontal line represents the average grain density of 2.71 g/cm³ for the complete data set. As the carbonate content increases, the grain density converges on the value of 2.77 g/cm³. The scatter in the grain density for low carbonate content reflects the varied samples, both basalt and sediment, and both clay and silica minerals in the sediments.

be somewhat offset by the fact that the siliceous samples tend to have higher porosities, whereas the carbonate samples tend to have lower porosities.

ACOUSTIC VELOCITY

An analysis of the acoustic velocity can be useful for future use in geophysical modeling and interpretation, as well as providing diagnostic information about lithologic variations. There have been numerous studies on the correlation of the acoustic velocity with porosity and lithology (e.g., Fulthorpe et al., 1989; Hamilton et al., 1982; Hamilton and Bachman, 1982; Mienert, 1984; Mienert et al., 1988; Nobes et al., 1986;

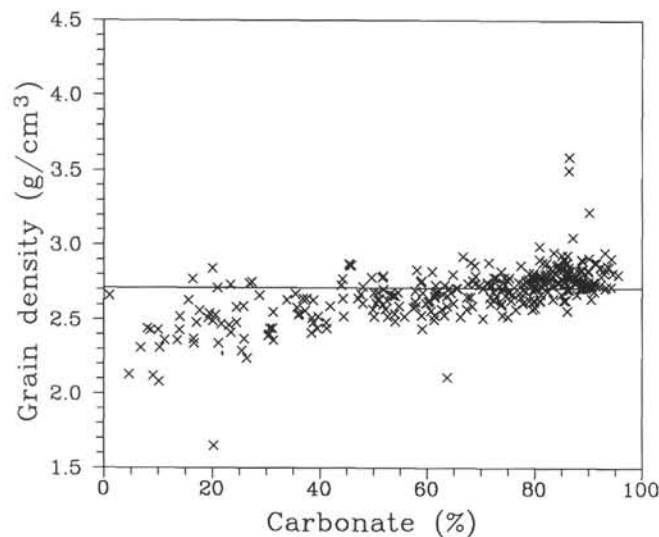


Figure 10. Grain density vs. carbonate content for Site 704. Note the general decrease in grain density for decreasing carbonate content resulting from the increased presence of low-density biogenic silica.

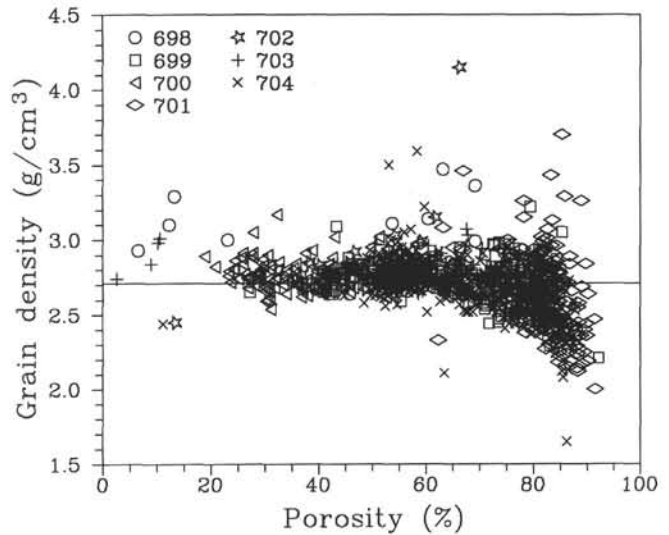


Figure 11. Grain density vs. porosity. The horizontal line represents the average grain density of 2.71 g/cm³. The downturn at high porosity is due to the siliceous oozes, which tend to have higher porosities and lower grain densities.

Nobes, 1989), especially the clay content (Nobes, 1989) and carbonate content (Hamilton et al., 1982; Mienert, 1984). In the past, both empirical (e.g., Castagna et al., 1985) and theoretical (e.g., Nafe and Drake, 1957) models have been fit to a given set of velocity vs. porosity (or density) data. Both sets of models have not been generally applicable. The empirical models tend to be highly dependent on the data set, and the theoretical equations are typically derived from a simplified and thus restricted physical model.

As an example, the Wood (1941) model is derived by assuming that the medium is composed of particles in fluid suspension, that is, a slurry. On the other hand, the Wyllie et al. (1956) time-average equation is based on a model of mixtures of rigid media. Both models are approximately valid at high (Wood) or low (Wyllie) porosities. If, however, we assume a medium to be composed of a mixture of slurry and

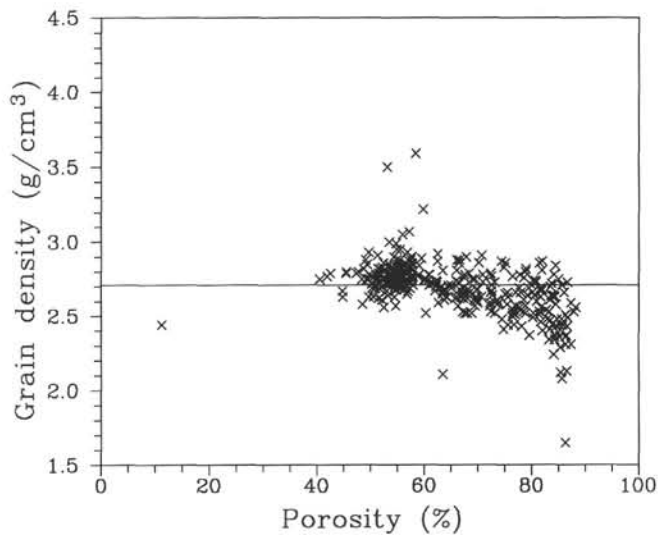


Figure 12. Grain density vs. porosity for Site 704. This plot reinforces the trends identified in Figures 9 through 11.

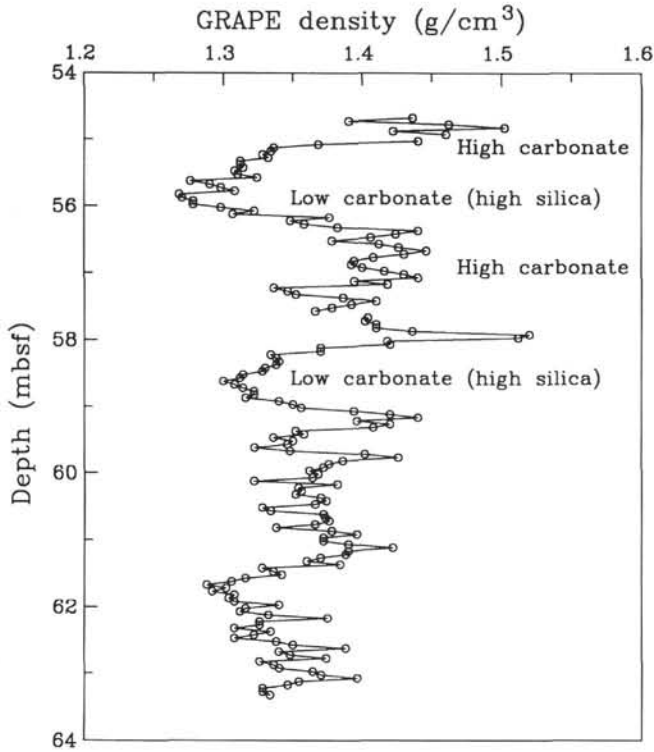


Figure 13. GRAPE density vs. depth for Core 114-704A-7H, illustrating the combined effects of lower grain density and high porosity on the density in intervals with high silica (low carbonate) (e.g., 55–56 and 58–59 mbsf). In contrast, intervals with a high carbonate content have higher grain density and generally lower porosity (e.g., above 55 and from 56.5 to 58 mbsf).

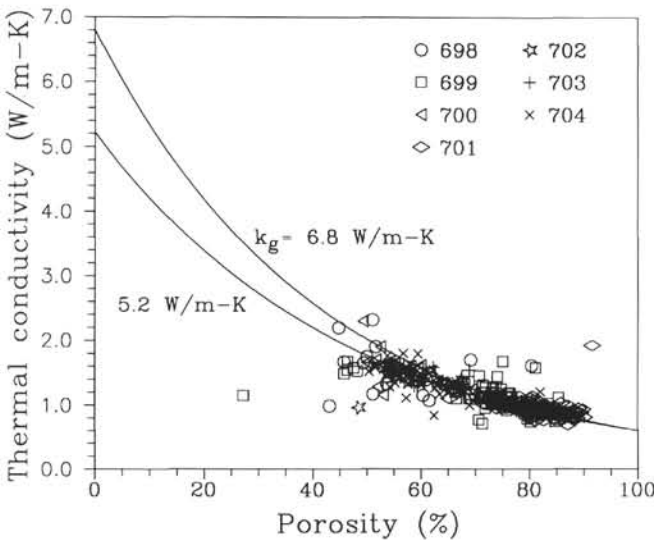


Figure 14. Thermal conductivity vs. porosity. The model curves use grain thermal conductivities of 5.2 and 6.8 W/m-K and a value of 0.6 W/m-K for water. Note the lack of resolution of the models at high porosity.

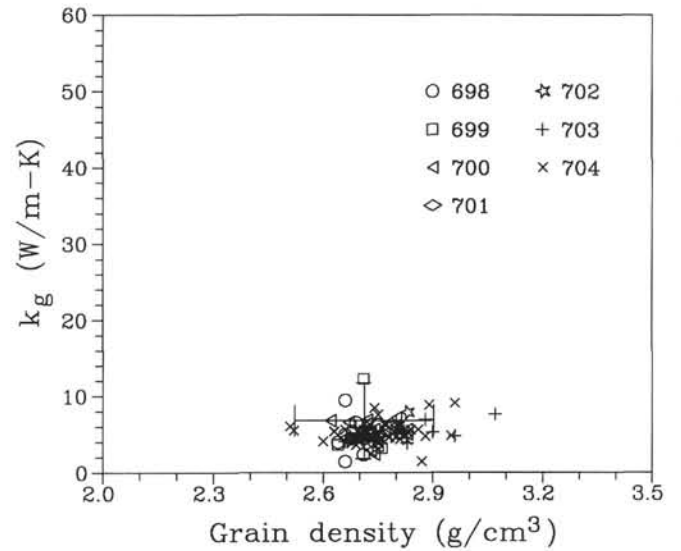


Figure 15. Grain thermal conductivity vs. grain density for carbonate content greater than 70%. The mean and one standard deviation error bars for the entire data set are plotted. Note the tight cluster of data points for the carbonate-rich samples at a higher grain density and slightly lower grain thermal conductivity.

rigid material, in proportion to the porosity, then we can derive a model that approaches the Wood and Wyllie models at the porosity extremes and lies somewhere between at moderate porosities (Nobes, 1989). Thus:

$$1/V_p = \phi/V_{Wood} + (1 - \phi)/V_{Wyllie},$$

where ϕ is the fractional porosity. Such a model has been found to fit well over a wide range of porosities.

The model proposed by Nobes et al. (1986) and Nobes (1989), as defined by the preceding equation, has been used

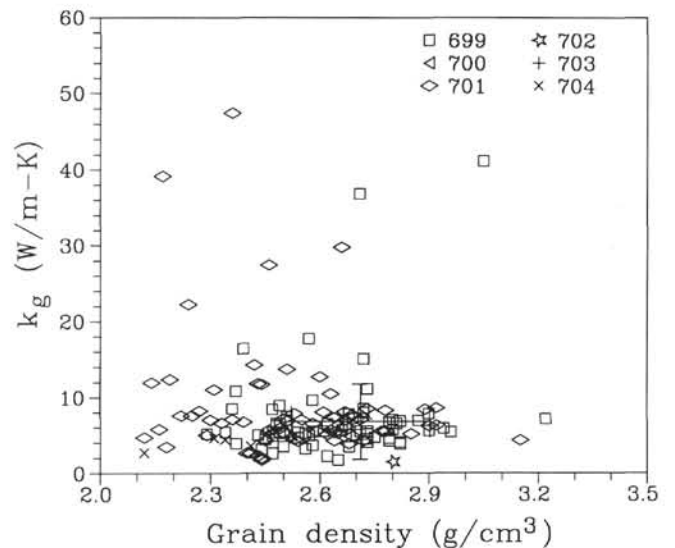


Figure 16. Grain thermal conductivity vs. grain density for samples with carbonate content less than 30%. The mean and one standard deviation error bars for the entire data set are plotted. Note the large scatter of data points with a greater concentration at lower grain density and higher grain thermal conductivity.

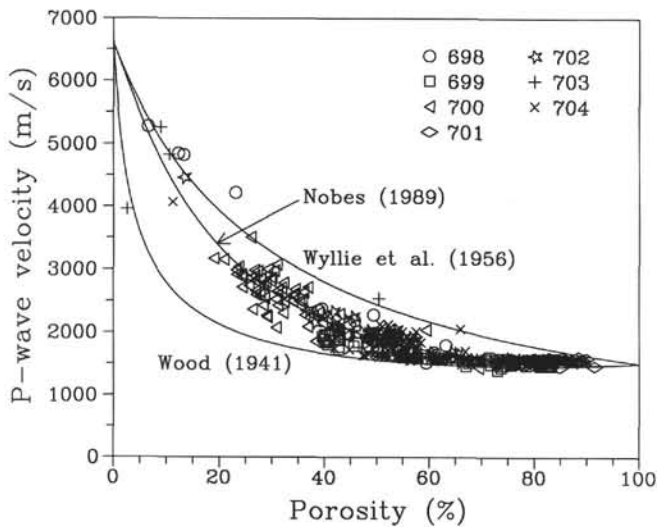


Figure 17. Compressional-wave velocity vs. porosity. The Wood (1941) and Wyllie et al. (1956) equations (bottom and top curves, respectively) provide approximate lower and upper limits on the velocity. The a priori model of Nobes et al. (1986) and Nobes (1989) (middle curve) fits the data well.

here to model the variation of the acoustic velocity with porosity, as shown in Figure 17. The grain matrix velocity has been taken to be that for calcite, 6600 m/s, the limiting case for carbonate, without allowing for the presence of silica, with a grain velocity of 6050 m/s, or clay, 3400 m/s. Nonetheless, the model curve passes through the clusters of data points, bounded above and below by the limiting cases of the Wyllie and Wood equations, respectively. The correlation coefficient is 0.88 and the rms error is 8.6%. If we allow the model lithology to vary, so that silica is assumed to make up the entire noncarbonate component of the grain material, then the correlation coefficient is 0.92 and the rms error is 8.5%, a marginal improvement in the fit.

The porosity decreases with increasing diagenesis, as noted previously, and the velocity reflects this. As shown in Figure 18, we can identify a definite diagenetic trend, from

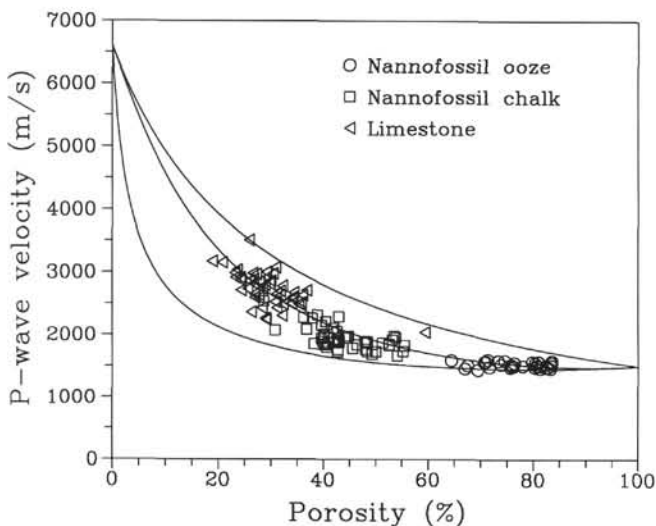


Figure 18. Compressional-wave velocity vs. porosity, illustrating the diagenetic trend from ooze to chalk to limestone. The data trend follows the model curve of Nobes et al. (1986) and Nobes (1989).

ooze to chalk to limestone, following the model curve. As the degree of diagenesis increases and the porosity decreases, the velocity increases accordingly.

SHEAR STRENGTH

Some general features were apparent when the shear-strength data were examined. For example, those data from sites with approximately "normal" sedimentation rates with little disturbance, Sites 698 to 701, tend to have a higher shear strength compared with data from Sites 703 and 704. The sedimentation rate at Site 704 was quite high, and Site 703 is located on the slope of a seamount and evidence of past mass flows exists in the Site 703 cores. Such comparisons are problematic, however, because we must question the validity of the shear-strength data for nonclay sediments (Craig, 1983).

CONCLUSIONS

The interrelationships of physical properties are controlled by the lithology and the degree of diagenetic compaction and cementation. As the carbonate content increases, the porosity, wet-bulk density, and acoustic velocity tend to increase as well. The grain density and grain thermal conductivity tend to converge on well-constrained values of $2.77 \pm 0.13 \text{ g/cm}^3$ and $5.2 \pm 1.5 \text{ W/m-K}$, respectively. As the degree of diagenetic cementation increases, the porosity and the acoustic velocity tend to increase. The velocity, in particular, closely follows a theoretical model curve as the sediment progresses from ooze to chalk to limestone. In addition to diagenesis, tectonism and depositional hiatuses influence the physical properties. The physical properties can be used as an aid in the classification of hiatuses as erosional or nondepositional.

ACKNOWLEDGMENTS

The work presented here was supported by a Collaborative Special Projects Grant from the Natural Sciences and Engineering Research Council of Canada. One of the authors (GJD) acknowledges the support of NSERCC through a Summer Research Assistantship award. Portions of the work benefitted from the comments of Drs. M.B. Dusseault and J.-M. Konrad. We thank the anonymous reviewers for their careful reading of the manuscript.

REFERENCES

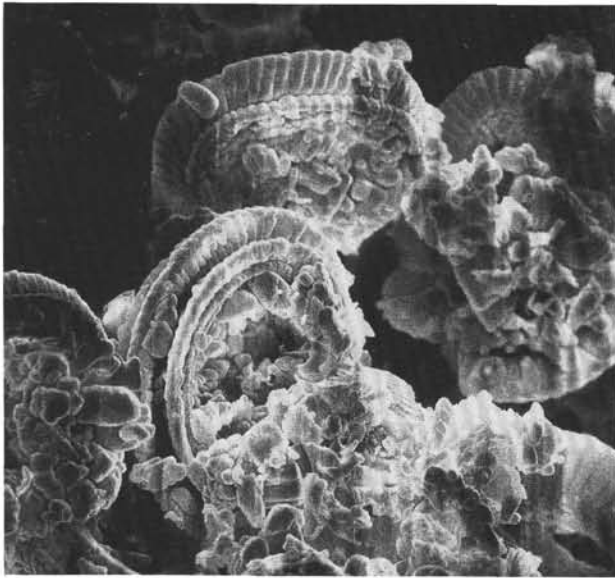
- Boyce, R. E., 1976. Definitions and laboratory techniques of compressional sound velocity parameters and wet-water content, wet-bulk density and porosity parameters by gravimetric and gamma-ray attenuation techniques. In Schlanger, S. O., Jackson, E. D., et al., *Init. Repts. DSDP*, 33: Washington (U.S. Govt. Printing Office), 931-958.
- _____, 1977. Deep Sea Drilling Project procedures for shear strength measurement of clayey sediment using modified Wykeham Farrance laboratory vane apparatus. In Barker, P., Dalziel, I.W.D., et al., *Init. Repts. DSDP*, 36: Washington (U.S. Govt. Printing Office), 1059-1068.
- Castagna, J. P., Batzle, M. L., and Eastwood, R. L., 1985. Relationships between compressional-wave and shear-wave velocities in clastic silicate rocks. *Geophysics*, 50:571-581.
- Craig, R. F., 1983. *Soil Mechanics*: Wokingham, Berkshire (Van Nostrand Reinhold).
- Fulthorpe, C. S., Schlanger, S. O., and Jarrard, R. D., 1989. In situ acoustic properties of pelagic carbonate sediments on the Ontong Java Plateau. *J. Geophys. Res.*, 94:4025-4032.
- Hamilton, E. L., and Bachman, R. T., 1982. Sound velocity and related properties of marine sediments. *J. Acoust. Soc. Am.*, 72:1891-1904.
- Hamilton, E. L., Bachman, R. T., Berger, W. H., Johnson, T. C., and Mayer, L. A., 1982. Acoustic and related properties of calcareous deep-sea sediments. *J. Sediment. Petrol.*, 52:733-753.

- Henderson, J., and Davis, E. E., 1983. An estimate of the heat flow in the western North Atlantic at Deep Sea Drilling Project Site 534. In Sheridan, R. E., Gradstein, F. M., et al., *Init. Repts. DSDP*, 76: Washington (U.S. Govt. Printing Office), 719-724.
- Johnson, G. R., and Olhoeft, G. R., 1984. Density of rocks and minerals. In Carmichael, R. S. (Ed.), *CRC Handbook of Physical Properties of Rocks* (vol. 3): Boca Raton, FL (CRC Press), 1-38.
- Mienert, J., 1984. The importance of carbonate content in the acoustic stratigraphy of Panama Basin. *Mar. Geol.*, 54:237-247.
- _____, 1986. Akustostratigraphie im äquatorialen Ostatlantik: zur Entwicklung der Tiefenwasserzirkulation der letzten 3.5 Millionen Jahre. "Meteor" *Forschungs-Ergebnisse, Reihe C*, 40:19-86.
- Mienert, J., Curry, W. B., and Sarnthein, M., 1988. Sonostratigraphic records from equatorial Atlantic deep-sea carbonates: paleoceanographic and climatic relationships. *Mar. Geol.*, 83:9-20.
- Nafe, J. E., and Drake, C. L., 1957. Variation with depth in shallow and deep water marine sediments of porosity, density and the velocities of compressional and shear waves. *Geophysics*, 22:523-547.
- Nobes, D. C., 1989. A test of a simple model of the acoustic velocity in marine sediments. *J. Acoust. Soc. Am.*, 86:290-294.
- Nobes, D. C., Villinger, H., Davis, E. E., and Law, L. K., 1986. Estimation of marine sediment bulk physical properties at depth from seafloor geophysical measurements. *J. Geophys. Res.*, 91:14033-14043.
- Shipboard Scientific Party, 1988a. Preliminary results of subantarctic South Atlantic Leg 114 Ocean Drilling Program. In Ciesielski, P. F., Kristoffersen, Y., et al., *Proc. ODP, Init. Repts.*, 114: College Station, Texas (Ocean Drilling Program), 797-803.
- _____, 1988b. Site 700. In Ciesielski, P. F., Kristoffersen, Y., et al., *Proc. ODP, Init. Repts.*, 114: College Station, Texas (Ocean Drilling Program), 255-361.
- van der Lingen, G. J., and Packham, G. H., 1975. Relationships between diagenesis and physical properties of biogenic sediments of the Ontong-Java Plateau (Sites 288 and 289, Deep Sea Drilling Project). In Andrews, J. E., Gradstein, F. M., et al., *Init. Repts. DSDP*, 30: Washington (U.S. Govt. Printing Office), 443-481.
- Von Herzen, R. P., and Maxwell, A. E., 1959. The measurements of thermal conductivity of deep-sea sediments by a needle probe method. *J. Geophys. Res.*, 65:1535-1541.
- Wood, A. B., 1941. *A Textbook of Sound*: New York (Macmillan).
- Woodside, W., and Messmer, J. H., 1961. Thermal conductivity of porous media. *J. Appl. Phys.*, 32:1688-1699.
- Wyllie, M.R.J., Gregory, A. R., and Gardner, L. W., 1956. Elastic wave velocities in heterogeneous and porous media. *Geophysics*, 21:41-70.

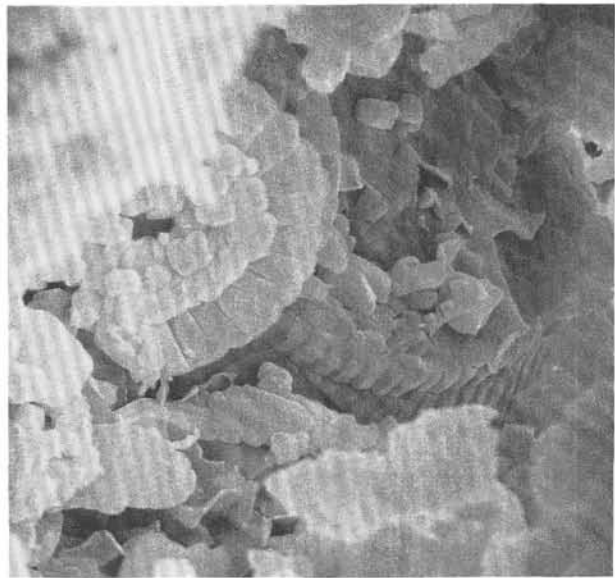
Date of initial receipt: 30 September 1988

Date of acceptance: 6 December 1989

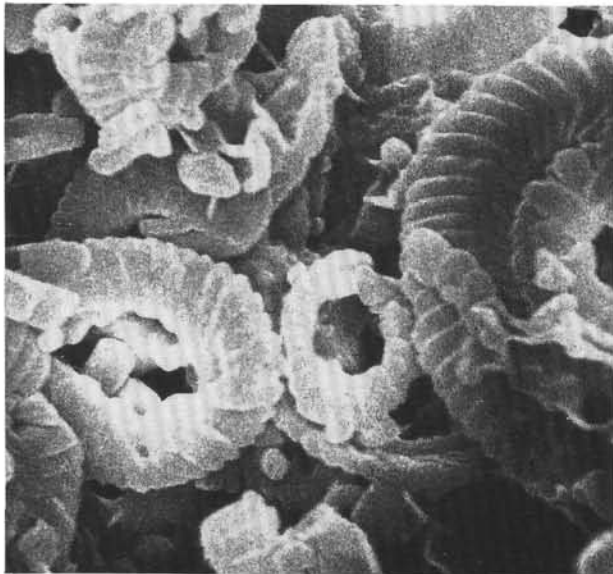
Ms 114B-162



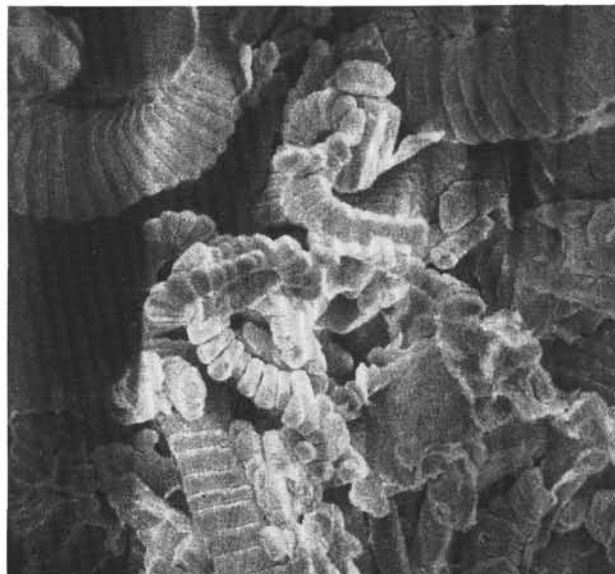
1 5 μ m



2 1 μ m



3 1 μ m



4 1 μ m

Plate 1. Scanning electron photomicrographs of samples of early middle Eocene age (approximately 45 Ma) from Sites 699 and 700. 1 and 2. Sample 114-699A-45X-6, 99–101 cm. Carbonate content = 75.2%, grain density = 2.73 g/cm³, and porosity = 44.8%. The overgrowth is readily apparent, indicative of dissolution and reprecipitation. 3 and 4. Sample 114-700B-9R-1, 100–102 cm. Carbonate content = 75.0%, grain density = 2.74 g/cm³, and porosity = 57.8%. There is much less evidence of dissolution and reprecipitation.